[American Journal of Science, Vol. 311, March, 2011, P. 211–236, DOI 10.2475/03.2011.02]

MINERAL REPLACEMENT REACTIONS IN SOLID SOLUTION-AQUEOUS SOLUTION SYSTEMS: VOLUME CHANGES, REACTIONS PATHS AND END-POINTS USING THE EXAMPLE OF MODEL SALT SYSTEMS

KILIAN POLLOK*,**, CHRISTINE V. PUTNIS**, and ANDREW PUTNIS**

ABSTRACT. The volume change of solid phases associated with dissolution and precipitation reactions during mineral replacement is a critical factor for the advancement of the reaction boundary. Contributing parameters to the overall volume change of a replacement reaction are the molar volume of parent and product and their solubility ratio within a given solution. Based on simple model salt systems, the contribution of solubility to volume change is quantitatively determined. For NaCl-KCl as an example of a binary salt system without solid solution, the relative volume changes can be calculated for various reaction paths using the slope of the solubility from a simple solubility diagram. For KBr-KCl as an example of a binary salt system with complete solid solution, the determination of the solubility curve is based on a modified Lippmann phase diagram called a solubility phase diagram. It allows a quantitative calculation of the relative volume change based on the solid solution-aqueous solution (SS-AS) relationships for variable solution compositions and reaction paths in the salt-water system. Reaction kinetics, textures and the compositional evolution of replacements in both salt systems can be conclusively explained by the relative volume change on the basis of experimentally constrained reaction paths. The analogy from simple model system to replacement reactions at the Earth's surface and crustal conditions (for example in apatites or feldspars) may offer insights to successfully describe volume changes and porosity generation in mineral reactions on the basis of solubility data towards a more quantitative modeling of interface-coupled dissolution-precipitation reactions.

Key words: SS-AS systems, Volume change, Solubility, Replacement, Dissolution-precipitation, Pseudomorphism

GLOSSARY OF SYMBOLS

a	activity
a_0, a_1, a_2	dimensionless coefficients to calculate solid-phase activity coefficients
f	activity coefficient of components in solid solution
m	molality
m_i^0	molality in pure AB or AC solution
n	amount of substance
n^{tot}	amount of substance of the total system (solid and aqueous solution)
q	stoichiometric coefficient defined by the absolute value of the slope of the solubility curve
s_{AB}, s_{AC}	solubility of AB and AC, respectively
s_{eq}	solubility in mol/kg
x	mole fraction
x^{tot}	mole fraction of the total system (solid and aqueous solution)
x_{AB}^{repl}	composition of replacement as mole fraction
K_{AB}, K_{AC}	solubility product of AB and AC, respectively
P_n	point n in the solubility and solubility phase diagram
V_M	molar volume
$\chi_{i,aq}$	activity fraction in aqueous solution

* Bayerisches Geoinstitut, Universität Bayreuth, D-95440 Bayreuth, Germany; kilian.pollok@uni-bayreuth.de
** Institut für Mineralogie, Universität Münster, Corrensstr. 24, D-48149 Münster, Germany

γ_i	aqueous activity coefficient
γ_i^0	aqueous activity coefficient in pure AB or AC solution
ξ	reaction extent variable
Δm	difference in molality
ΔV^r	relative volume change
$\Sigma\Pi$	total solubility product variable
$\Sigma\Pi_{eq}$	total solubility product at equilibrium
Ψ	empirical exponent
$[A^+]$, $[B^-]$, $[C^-]$	activity of ions in aqueous solution

Subscripts

$i = A^+, B^-, C^-$	ions in aqueous solution
AB, *AC*	components in solid solution
d, *p*	dissolved and precipitated, respectively

INTRODUCTION

The replacement of one mineral by another is an important and striking phenomenon of mineral reactions in many geological environments and was already described in the 19th century (Blum, 1843). Thereby, the new mineral, although chemically and/or structurally different from the parent mineral, occupies the space and crystallographic characteristics of the former mineral. Often, such pseudomorphs are recognized by preserving the euhedral shape of the former mineral. Although there are various scenarios for replacement reactions, we focus here on the replacement of an isostructural mineral by another, for example when they form a solid solution. Natural and experimental examples of such replacements are manifold in many mineral groups such as apatite (Yanagisawa and others, 1999; Rendón-Angeles and others, 2000a, 2000b, 2000c; Harlov and others, 2002, 2005; Harlov and Förster, 2003; Seydoux-Guillaume and others, 2007), feldspars (O'Neil and Taylor, 1967; Walker and others, 1995; Labotka and others, 2004; Putnis and others, 2007a; Engvik and others, 2009; Niedermeier and others, 2009; Parsons and Lee, 2009; Hövelmann and others, 2010), sulfides (Ramdohr, 1980; Tenailleau and others, 2006; Xia and others, 2009), pyrochlore (Geisler and others, 2004, 2005a, 2005b), zircon (Tomaschek and others, 2003; Spandler and others, 2004; Geisler and others, 2007; Rubatto and others, 2008; Kusiak and others, 2009; Soman and others, 2010) and garnet (Pollok and others, 2008). They are commonly characterized by a sharp replacement front and have been described in terms of an interface-coupled dissolution-reprecipitation mechanism (Putnis and Putnis, 2007; Putnis, 2009). Furthermore, a similar mechanism has been reported as a mechanism for glass corrosion (Geisler and others, 2010).

The preservation of the outer shape and, therefore, external volume of the replaced crystal is a prerequisite to create a pseudomorph. The textural inheritance implies that the rates of dissolution and precipitation are somehow coupled at the reaction interface (see discussion in Putnis, 2009).

Ferry (2000) considered the molar volume change of the replacement reaction and the force of crystallization, which is the force exerted by stresses resulting from crystal growth. He concluded that a negative molar volume change as often observed in retrograde mineral reactions is a relevant factor in stabilizing the replacing mineral. In general, volume changes associated with mineral reactions are of great importance in terms of the kinetics of re-equilibration. A volume decrease has the ability to produce a "reaction enhanced" permeability (Rumble and Spear, 1983; Cartwright, 1997; Jamtveit and others, 2000), allowing replacement reactions to create pathways for fluid through minerals (Putnis and John, 2010) and, therefore, might trigger and catalyze metamorphic reactions. In fact, microporosity has been recognized in many cases [for example the replacement of leucite by analcime (Putnis and others, 1994, 2007b);

cryptoperthite to coarse patch perthite (Walker and others, 1995; Parsons and Lee, 2009); chloro-, hydoxy-, fluoroapatite system (Yanagisawa and others, 1999; Rendón-Angeles and others, 2000a, 2000b, 2000c)], but porosity development cannot be explained simply by changes in molar volume of the reactants.

The solubility of the solid phases is generally affected by a number of variables, for example, fluid composition, temperature, pressure, pH, grain size, and for solid solutions by composition. The initial conditions for replacement reactions and the fluid compositions in natural systems are usually unknown. Therefore, the NaCl-KCl-H_2O and the KBr-KCl-H_2O systems have been chosen as model systems because of their relative simplicity (structurally and experimentally) and the availability of thermodynamic data. Experiments on replacement reactions in the KBr-KCl-H_2O system show both negative and positive volume changes with significantly different replacement textures (Putnis and Mezger, 2004; Putnis and others, 2005). Similar replacement textures have been reported for various soluble salt solid solutions (Glikin, 2008). Since the compositional changes during the replacement strongly depend on the solution composition, solid solution-aqueous solution (SS-AS) reaction paths have to be considered for a quantitative determination of the associated volume changes.

In this paper, the use of solubility diagrams is illustrated for the case of salt-water systems without solid solution (NaCl-KCl) and relevant terms regarding the volume changes will be introduced. The conceptual model for the dissolution-precipitation reaction in this system has been outlined by Putnis (2002) but will be presented here quantitatively in relation to solubility at equilibrium. The description is then extended to systems with complete binary solid solution (KBr-KCl). In this latter case, equilibrium states in SS-AS systems are represented in a modification of Lippmann phase diagrams (Lippmann, 1980), the solubility phase diagram, which consistently links the solubility diagram with the thermodynamic SS-AS description. General equations for reaction paths and the associated volume changes will be related.

Replacement and volume change in the NaCl-KCl-H_2O system

Here we present a generalized reaction formula for systems without substitutional miscibility, which allows the volume changes of solid phases to be quantified.

Solubility and Equilibrium

Solubility diagrams are frequently used to visualize experimental solubility data in salt-water systems at a fixed temperature (for example Silcock, 1979). In figure 1 the change of the solubility for one component (KCl) depending on the amount of the second component (NaCl) due to the common ion effect is shown. For systems with almost no solid solution such as NaCl-KCl under ambient conditions, each point on the solubility curve represents the composition of a saturated solution with respect to one solid, either NaCl or KCl. At the isothermal invariant point E (eutonic point) the solution is saturated with respect to both solid phases. The intersections with the X and Y axis are the solubilities of pure NaCl and pure KCl in water at 25 °C, respectively. Points below the curve represent undersaturated solutions, points above it are supersaturated with respect to a solid phase.

Reaction Paths and Volume Changes

A dissolution-precipitation reaction path of an initial NaCl crystal in an undersaturated mixed solution (P_0) is illustrated in figure 1. The dissolution of NaCl (P_0 to P_1) leads to an intersection with the solubility curve (P_1) where the solution is saturated with respect to KCl. The initial NaCl crystal is still not in equilibrium with the solution but further dissolution of NaCl must now be accompanied by the precipitation of KCl, which is the thermodynamically stable solid. The dissolution-precipitation reaction (KCl precipitates, NaCl dissolves) changes the composition of the solution, which

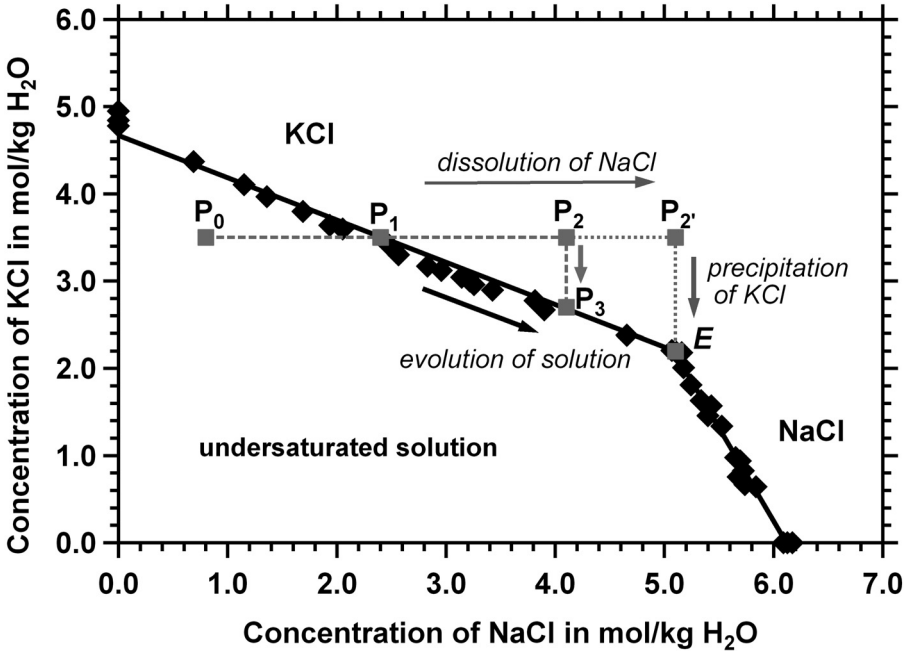

Fig. 1. The solubility diagram for NaCl-KCl at 25 °C. The experimental solubility data (diamonds) from Silcock (1979) has been regressed linearly (from $m_{NaCl} = 0$ to E: $y = 4.67-0.485x$; from $m_{NaCl} = E$ to m_{max}: $y = 13.093-2.141x$). A dissolution-precipitation path for NaCl dissolution and KCl precipitation is shown.

therefore approaches the eutonic point E. At this point, NaCl will not dissolve further because the saturated solution is in thermodynamic equilibrium with respect to both NaCl and KCl. The reaction can be expressed in terms of mass-balance as:

$$\mathrm{NaCl} + q\mathrm{K}^+ \rightarrow q\mathrm{KCl} + (1-q)\mathrm{Cl}^- + \mathrm{Na}^+ \qquad (1)$$

where the coefficient $q = \left|\frac{\Delta m_{K,aq}}{\Delta m_{Na,aq}}\right|$ accounts for the change in solubility as a function of solution composition, which is equivalent to the value of the slope of the solubility curve. In the case of the NaCl-KCl-H_2O system the solubility curve can be described linearly. Thus, the linear slope also represents the ratio of precipitated (n_p) to dissolved (n_d) material and is constant throughout the reaction $\left(q = \left|\frac{\Delta m_{K,aq}}{\Delta m_{Na,aq}}\right| = \frac{n_p}{n_d}\right)$. There is a virtual one-step dissolution/precipitation path from P_1 via P_2 to P_3 or P_1 via $P_{2'}$ to E. Note that the real reaction path may never reach point P_2 if a certain (lower) supersaturation leads to nucleation and precipitation of a solid phase but the mass balance will not be affected. Using the linearly regressed solubility data for the NaCl-KCl-H_2O system from Silcock (1979) the reaction can be written as

$$1\ \mathrm{NaCl} + 0.485\ \mathrm{K}^+ \rightarrow 0.485\ \mathrm{KCl} + 0.515\ \mathrm{Cl}^- + 1\ \mathrm{Na}^+. \qquad (2)$$

The stoichiometric coefficients for the solute species are given in mol/kg H_2O in a saturated solution. Note that the ratio of dissolved NaCl to precipitated KCl is given by the absolute value of the slope, which is determined by the solubility curve alone.

To calculate a volume change from this reaction the molar volumes of the solid phases have to be taken into account. The relative volume change ΔV^r is given by:

TABLE 1

Volume changes calculated for the NaCl-KCl-H_2O and KBr-KCl-H_2O system using equations (3) and (18), respectively

Dissolved phase	Molar volume [cm^3/mol]	Starting solution saturated with respect to	Precipitated phase	Molar volume [cm^3/mol]	Final solution composition	Volume change ΔV^r [%]
NaCl	27.06	KCl	KCl	37.46	$x_{Na,\,aq} \leq 0.70$	-32.9
KCl	37.46	NaCl	NaCl	27.06	$x_{Na,\,aq} \leq 0.70$	-66.3
KBr	43.27	KCl	$KBr_{0.9}Cl_{0.1}$	42.69	$x_{Br,\,aq} = 0.823$	-4.3
KBr	43.27	KCl	$KBr_{0.9}Cl_{0.1}$	42.69	$x_{Br,\,aq} = 0.823$	+0.8 local
KBr	43.27	KCl	$KBr_{0.5}C_{l0.5}$	40.36	$x_{Br,\,aq} = 0.594$	-27.1
KBr	43.27	KCl	$KBr_{0.5}C_{l0.5}$	40.36	$x_{Br,\,aq} = 0.594$	-14.3 local
KBr	43.27	KCl	$KBr_{0.1}Cl_{0.9}$	38.04	$x_{Br,\,aq} = 0.350$	-43.1
KBr	43.27	KCl	$KBr_{0.1}Cl_{0.9}$	38.04	$x_{Br,\,aq} = 0.350$	-44.2 local
KCl	37.46	KBr	$KBr_{0.9}Cl_{0.1}$	42.69	$x_{Br,\,aq} = 0.823$	-10.35
KCl	37.46	KBr	$KBr_{0.9}Cl_{0.1}$	42.69	$x_{Br,\,aq} = 0.823$	-7.9 local
KCl	37.46	KBr	$KBr_{0.5}C_{l0.5}$	40.36	$x_{Br,\,aq} = 0.594$	-1.3
KCl	37.46	KBr	$KBr_{0.5}C_{l0.5}$	40.36	$x_{Br,\,aq} = 0.594$	+16.3 local
KCl	37.46	KBr	$KBr_{0.1}Cl_{0.9}$	38.04	$x_{Br,\,aq} = 0.350$	+2.1
KCl	37.46	KBr	$KBr_{0.1}Cl_{0.9}$	38.04	$x_{Br,\,aq} = 0.350$	+2.7 local

Molar volumes are derived from the molar mass and calculated density of the salts.

$$\Delta V^r\,[\%] = \frac{n_p V_{M,p} - n_d V_{M,d}}{n_d V_{M,d}} \cdot 100 = \frac{n_p V_{M,p}}{n_d V_{M,d}} \cdot 100 - 100 = q \cdot \frac{V_{M,p}}{V_{M,d}} \cdot 100 - 100. \qquad (3)$$

The ΔV^r for the replacement of NaCl by KCl calculated from solubility data is -33 percent (table 1). This volume change is independent of the reaction path chosen assuming that equilibrium between solid and solution is reached at the end of the reaction [two solids (for example KCl and NaCl) at the eutonic point]. Note that ΔV^r is significantly negative although the molar volume of KCl is higher than that of NaCl. The reason for this is due to the higher solubility of NaCl over KCl (at 25 °C), which results in a higher amount of NaCl dissolving than KCl precipitating.

The opposing reaction of KCl to NaCl leads to a ΔV^r of -66 percent. Both the molar volume and the difference in solubility contribute to the decrease of the relative volume. From the solubility data the reaction can be expressed as:

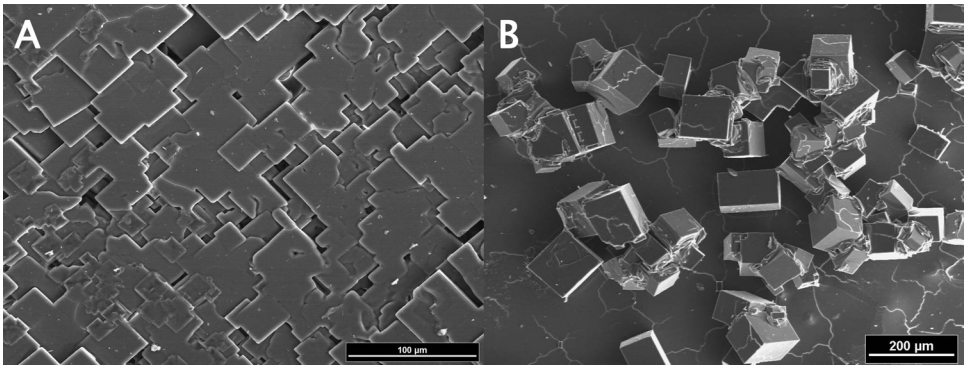

Fig. 2. SEM image of (A) a replaced surface of a NaCl crystal in KCl solution and (B) secondary NaCl crystals on a KCl surface partly dissolved in NaCl solution.

$$1\ KCl + 0.467\ Na^{+} \rightarrow 0.467\ NaCl + 0.533\ Cl^{-} + 1\ K^{+}. \quad (4)$$

Note that the reciprocal value of the slope must be taken from the solubility diagram with the concentrations of NaCl on the x axis and KCl on the y axis, respectively.

The temperature dependence of salt solubility can be quite variable. Farelo and others (1993) presented solubility diagrams at 25, 50 and 90 °C for NaCl and KCl in water as well as for the ternary system. NaCl shows only slight increase in solubility by 7 percent from 25 to 90 °C while an increase in solubility of 50 percent is found for KCl over the same temperature range. What are the consequences for the volume change of a replacement reaction in the ternary system? Essentially, the shape of the solubility diagram does not change significantly with temperature, only the position of the eutonic point is shifted. Consequently, the slopes of the solubility curves do not change and therefore, the volume change during a dissolution-precipitation reaction will be not affected. This result may be surprising at first glance, but it nicely illustrates that it is not the absolute solubility of the end-members that is important, but the changes of solubility for various solution compositions.

Comparison with Experimental Observations

Although this paper mainly deals with the effect of solubility on volume changes from a thermodynamic point of view, simple replacement experiments were conducted to ensure that the main results of the calculations are reasonable. A full description of the experimental procedure can be found in Putnis and Mezger (2004). In general, replacement reactions were initiated by placing a drop (a few μL) of solution saturated with respect to one end-member on a freshly cleaved ⟨100⟩ surface of the other end-member (for example placing a drop of a saturated KCl solution onto a NaCl crystal). After several minutes the solution on the crystal surface was soaked up quickly (to avoid precipitation on the surface) with a filter paper. All experiments were carried out at room temperature. The replaced surfaces were imaged by scanning electron microscopy (JEOL 8600 MXA).

NaCl substrate in KCl solution.—The replacement of NaCl in a KCl-saturated solution produces a crystallographically oriented rim of KCl which has a significant porosity. A secondary electron image of the replaced surface is given in figure 2A. The pores are terminated by straight crystal faces that resemble the crystallographic orientation of the original NaCl crystal. Such topotactic replacement reaction have been described for a number of systems (Yanagisawa and others, 1999; Putnis and

Mezger, 2004; Geisler and others, 2005b). The observation of porosity is in line with the calculated negative volume change.

KCl substrate in NaCl solution.—In the reverse experiment crystals of NaCl precipitate from a saturated NaCl solution in contact with a KCl crystal. The precipitation is initiated by the dissolution of KCl up to the required supersaturation. The newly formed crystals grow onto the surface of KCl and share no distinct crystallographic orientation with the substrate nor do they form a uniform layer (fig. 2B). Such an observation can also be understood in terms of the ΔV^r calculation. The relative volume change for this reaction is large and negative because both the molar volume and the solubility act in the same direction. As a consequence the relative volume decrease is too high to form a continuous layer of NaCl.

The different textures of the precipitated crystals (porous replacement layer versus individual crystals on the dissolving surface) may be qualitatively understood using percolation theory and energetic arguments. A negative ΔV^r (as porosity) affects the continuous 2D growth of the precipitate at the reacting surface. If we assume interpenetrating, but aligned square-like (2D) and cube-like (3D) pores as visible in figure 2A, the percolation threshold p_c is given as 66.7 percent and 27.7 percent, respectively (Baker and others, 2002). The percolation threshold describes the critical volume of pores at which an interconnected (2D/3D) layer of precipitate can no longer form. For the replacement of NaCl by KCl, a pore volume of 33 percent was calculated. This value is well below the 2D percolation threshold and allows the formation of a continuous, but porous KCl (mono-)layer on the NaCl substrate. However, the pore volume is higher than the 3D percolation threshold for cube-like pores, which means that the formation of a continuous replacement might not be possible. In fact, the replaced surface shows stacked layers of replacement, which may represent 2D nucleation at various sites rather than a continuous 3D replacement. An accurate determination of the porosity in the experiment is difficult and is furthermore complicated by the fact that the pore size may coarsen and partly or fully anneal out on the way to attaining textural equilibrium which follows the chemical equilibration (Putnis and others, 2005). For the reaction of saturated NaCl solution with the KCl substrate the calculated pore volume of 66 percent is already close to the 2D percolation threshold. Consequently, the NaCl precipitate forms single crystals rather than a highly porous replacement layer that would be energetically unfavorable due to the contribution of surface energy. These examples illustrate that the relative volume changes mark boundary conditions at which replacement reactions and pseudomorphism can take place, but further research is needed to validate these ideas.

REPLACEMENT AND VOLUME CHANGE IN THE KBr-KCl-H_2O SYSTEM

Solubility and Equilibrium

KBr and KCl form a complete solid solution. In such systems every point on the solubility curve (fig. 3A), that is, any composition of a saturated solution, is in equilibrium with a certain solid solution composition. Thus, the dissolution-precipitation paths cannot be simply deduced from the solubility diagram alone, because there is no information about the solid phase and its composition in such a diagram. A Lippmann phase diagram can be used to visualize SS-AS equilibrium states (Lippmann, 1977, 1980; Glynn and Reardon, 1990; Putnis and others, 1995; Glynn, 2000; Prieto, 2009) and the thermodynamic framework is given below.

Lippmann phase diagram.—Thermodynamic equilibrium in a SS-AS system with binary solid solution is defined by:

$$[A^+][B^-] = K_{AB}a_{AB} = K_{AB}x_{AB}f_{AB} \quad \text{and} \quad [A^+][C^-] = K_{AC}a_{AC} = K_{AC}x_{AC}f_{AC}. \qquad (5)$$

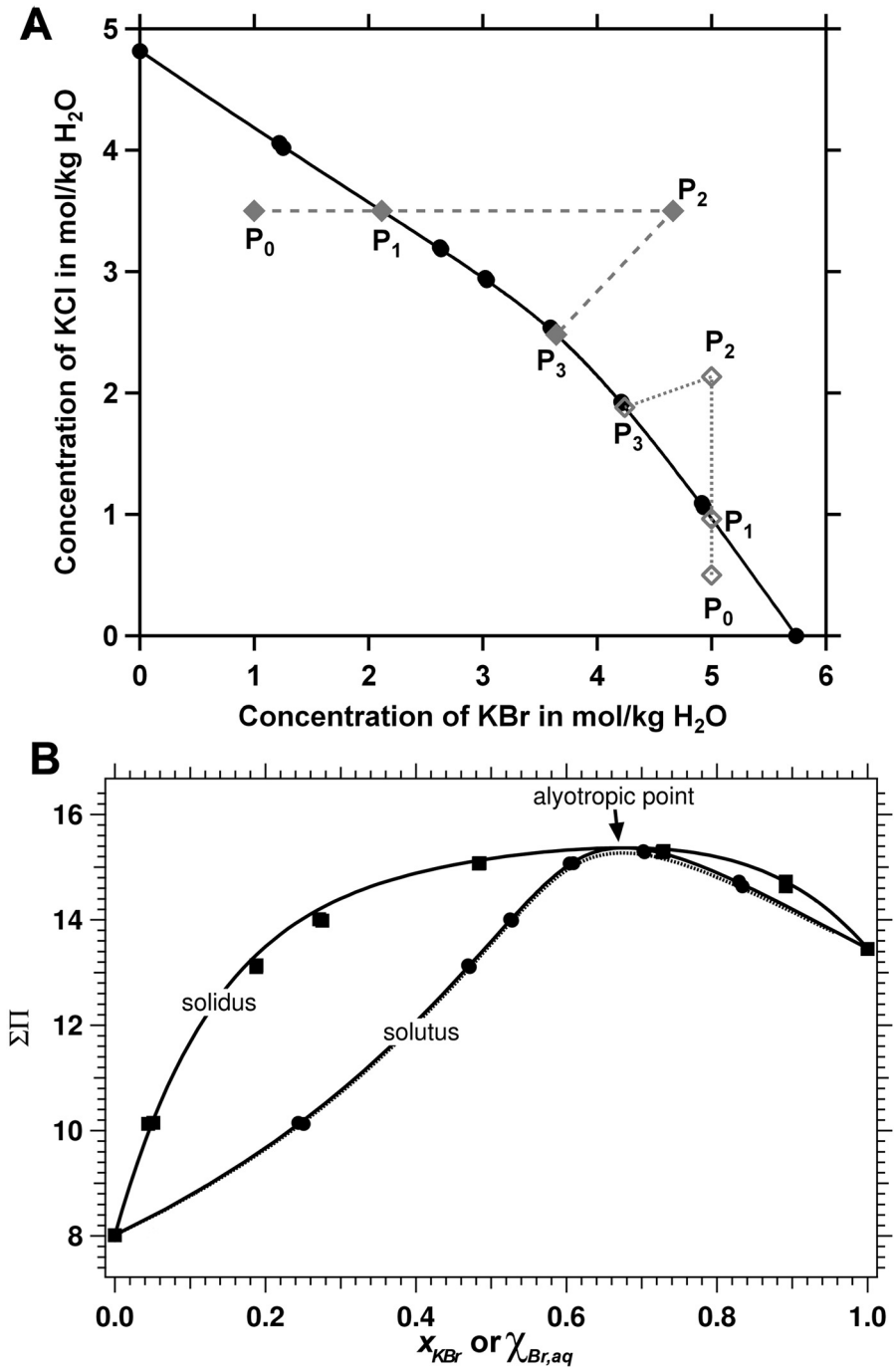

Fig. 3. (A) Solubility diagram of the KBr-KCl-H_2O system at 25 °C based on the data of Durham and others (1953). Black circles represent aqueous compositions in equilibrium with mixed solids from their experimental runs. The black curve is equivalent to the solutus curve of the solubility phase diagram and is constructed by equations (A15) and (A16). Two reaction paths are indicated in gray. Full diamonds show the dissolution of KBr in a mixed solution, open diamonds mark points for the dissolution of KCl in a mixed solution. Both reaction paths involve the precipitation of a mixed solid with a composition which is in equilibrium with P_3. Details of the paths are described in the text. (B) Lippmann diagram for the KBr-KCl-H_2O SS-AS system based on the data of Durham and others (1953). Pairs of black circles and squares represent aqueous and solid compositions in equilibrium. Solid lines are the solidus and solutus curve computed with solid-phase non-ideality parameters of $a_0 = 1.40$ and $a_1 = -0.08$. The dotted curve (nearly indistinguishable from the solutus curve) represents the solutus curve of the solubility phase diagram (fig. 4) converted to the Lippmann diagram using PHRQPITZ.

In SS-AS systems equilibrium is represented by two curves: the "solidus" and the "solutus" express the "total solubility product" variable, ΣΠ, as a function of solid composition and aqueous activity, respectively. The "total solubility product" variable was introduced by Lippmann (1977, 1980, 1982) as

$$\Sigma\Pi = [A^+]([B^-] + [C^-]). \tag{6}$$

At equilibrium the total solubility product as functions of the solid composition and the aqueous activity, respectively, is:

$$\Sigma\Pi_{eq} = K_{AB}x_{AB}f_{AB} + K_{AC}x_{AC}f_{AC} \quad (solidus) \tag{7}$$

and

$$\Sigma\Pi_{eq} = \frac{1}{\left(\frac{\chi_{B,aq}}{K_{AB}f_{AB}} + \frac{\chi_{C,aq}}{K_{AC}f_{AC}}\right)} \quad (solutus). \tag{8}$$

The aqueous *activity* fractions are given by:

$$\chi_{B,aq} = \frac{[B^-]}{([B^-] + [C^-])} \quad \text{and} \quad \chi_{C,aq} = \frac{[C^-]}{([B^-] + [C^-])} \tag{9}$$

Regular and sub-regular solid solution behavior can be considered by introducing solid-phase activity coefficients f_{AB} and f_{AC} with the form of an expansion series (Guggenheim, 1937; Redlich and Kister, 1948):

$$ln\ f_{AB} = x_{AC}^2[a_0 - a_1(3x_{AB} - x_{AC}) + a_2(x_{AB} - x_{AC})(5x_{AB} - x_{AC}) + \cdots] \tag{10}$$

and

$$ln\ f_{AC} = x_{AB}^2[a_0 - a_1(3x_{AC} - x_{AB}) + a_2(x_{AC} - x_{AB})(5x_{AC} - x_{AB}) + \cdots], \tag{11}$$

where a_i are dimensionless coefficients. Regular solid solutions can be described by a_0 alone whereas both a_0 and a_1 are needed to describe a subregular solid solution (Glynn, 2000).

$\Sigma\Pi_{eq}$ is the value of the ΣΠ variable which defines equilibrium for a given solid-solution composition. In the Lippmann phase diagram (fig. 3B, for KBr-KCl) the ΣΠ variable is represented on the ordinate whereas on the abscissa both the mole fraction of the solid and the aqueous activity fraction are given on a double scale. The solutus curve represents saturated solutions that are in equilibrium with a corresponding solid composition on the solidus curve. Horizontal tie-lines connect aqueous solution and solid solution compositions at equilibrium.

Experimental solubility data with a coexisting solid solution-aqueous solution for the KBr-KCl-H_2O system have been published by Durham and others (1953). The Lippmann phase diagram was calculated using equations (7) and (8) with the endmember solubility products of 13.46 ($10^{1.129}$) for KBr and 8.02 ($10^{0.904}$) for KCl. The solid-phase non-ideality parameters ($a_0 = 1.40$, $a_1 = -0.08$) have been fitted by Glynn and others (1990) to the data of Durham and others (1953) using the PHRQPITZ aqueous speciation model (Plummer and others, 1988) to calculate the aqueous activities of K^+, Br^-, and Cl^-. Both the solubility curve of the solubility diagram *and* the solutus curve of the Lippmann diagram (figs. 3A and 3B, respectively) represent saturated solutions. Thus, every point on the solutus curve corresponds to a unique point on the solubility curve. Therefore, the fitting of the solutus curve also determines the solubility curve and vice versa. Unfortunately, no analytical expression of the solubility curve can be directly obtained from the solutus curve for the following

reasons. Firstly, activities of the species in solution can only be determined with the assumption of $[A^+] = [B^-]+[C^-]$ which may be true for some solutions but not generally. Secondly, from known activities of the species in solution one cannot simply calculate the concentrations of the elements because the ionic strength of the solution is not known *a priori*. An inverse numerical procedure may overcome this problem (Kulik, 2006), however, it does not provide a self-consistent formulation for both diagrams.

Solubility phase diagram.—In the following section, a modification of the Lippmann model is presented which uses experimental solubility data and does not require the calculation of aqueous activity. It provides internally consistent expressions for the solubility and the solutus curve at the cost of introducing an additional empirical parameter that has to be fitted for every AB-AC-H_2O system.

The molality of A^+, m_{A^+}, in solution is equal to the total solubility when the condition $m_{A^+} = m_{B^-} + m_{C^-}$ is fulfilled. Such a condition can be easily reached experimentally by the dissolution of AB and AC solids to reach saturated solutions. With this assumption, an analogue to the solidus in the Lippmann model can be formulated (derivation and validation see Appendix A1):

$$s_{eq} = m_{A^+,eq} = \sqrt[\Psi]{s_{AB}^{\Psi} x_{AB} f_{AB} + s_{AC}^{\Psi} x_{AC} f_{AC}}. \tag{12}$$

Equally there is an analogous expression of the solutus:

$$s_{eq} = \sqrt[\Psi]{\frac{1}{\left(\frac{x_{B,aq}}{s_{AB}^{\Psi} f_{AB}} + \frac{x_{C,aq}}{s_{AC}^{\Psi} f_{AC}}\right)}}. \tag{13}$$

It is important to note that the empirical parameter Ψ does not represent any specific speciation or solution model. It can only be applied to solutions where the activities of the relevant species change gradually and continuously with increasing concentration as in most simple salt systems. Although it is thus more limited than a Lippmann diagram it can provide valuable insights into the complexity of coupled dissolution-precipitation reactions involving solid solutions.

Azimov and Shtukenberg (2000) report exponents of Ψ in the range of 1.5 to 2.5 for various systems of highly soluble salts. Note that these authors have used a different expansion series to describe the activities for non-ideal (subregular) solid solutions. To make the results of the Lippmann model and the solubility phase diagram as comparable as possible, the expressions shown in equations (10) and (11) as reported by Glynn and others (1990) are used. Using different forms for the solid-phase activity coefficient naturally affects the value of the exponent Ψ.

In order to construct the solubility phase diagram the best fit to the experimental data was achieved with an exponent of $\Psi = 2.35$ and non-ideality parameters of $a_0 = 1.36$ and $a_1 = -0.10$ using endmember solubilities of 5.74 mol/kg H_2O for KBr (s_{KBr}) and 4.82 mol/kg H_2O for KCl (s_{KCl}). The non-ideality parameters obtained are very close to those of the Lippmann model and should, in fact, give identical values since both models differ only in the treatment of the aqueous speciation. Therefore, the non-ideality parameters of the Lippmann model ($a_0 = 1.40$; $a_1 = -0.08$) fitted by Glynn and others (1990) were used and held constant during fitting, which results in $\Psi = 2.42$ with no significant decrease in goodness of fit. Note, that the constructed solubility phase diagram (fig. 4) has a similar topology to the Lippmann diagram (fig. 3B) but significantly different axes as it uses solubility and mole fractions. Converting the solubility curve back into the Lippmann phase diagram (using PHRQPITZ) gives an excellent match to the Lippmann solutus curve and confirms the applicability of the solubility phase diagram to such simple non-ideal SS-AS systems.

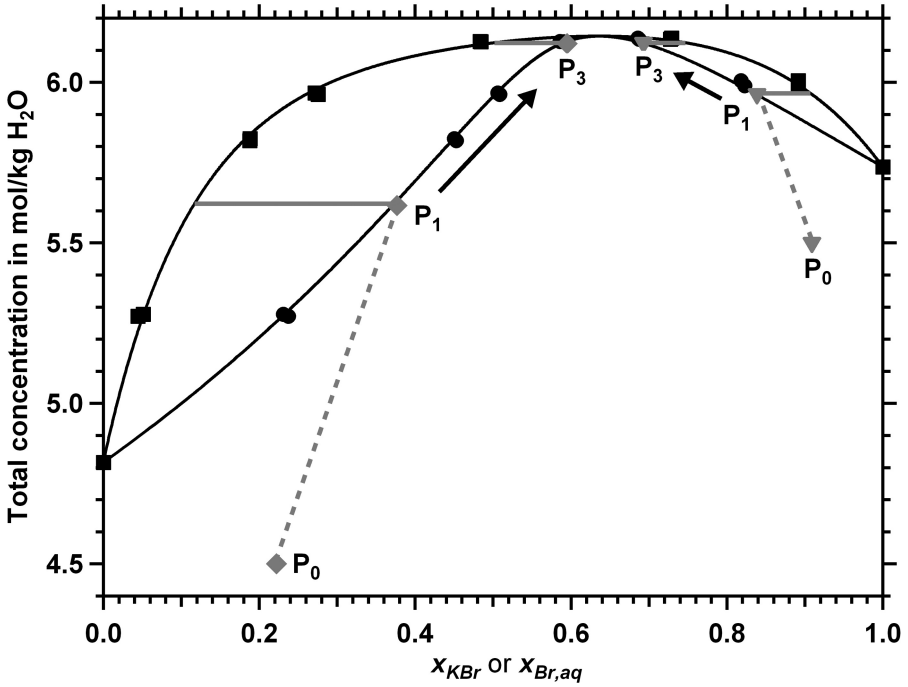

Fig. 4. Solubility phase diagram of the KBr-KCl-H_2O system. Experimental data is given as squares and circles and solid lines represent the solidus and solutus as in the Lippmann diagram (fig. 3B). The reaction paths are the same as in figure 3A. P_1 represents the starting point and P_3 the endpoint of the replacement reaction. P_2 is not shown because it is only used for the mass balance calculation but can not be reached in a real solution.

Reaction Path and Volume Changes

The dissolution-precipitation path within the KBr-KCl-H_2O system is more difficult to describe than for a system with no solid solution because the composition of the solid that precipitates is a function of solution composition that will be altered during dissolution. On the basis of the reaction path in the NaCl-KCl-H_2O system a dissolution-precipitation path can be formulated in the solubility diagram (fig. 3A) as well as the solubility phase diagram (fig. 4) of the KBr-KCl-H_2O system. Starting with an undersaturated mixed solution at P_0 in contact with a pure KBr crystal (dashed line in fig. 3A and fig. 4, an analogous path is indicated by a dotted line with KCl as starting crystal) the solution will eventually reach saturation by the dissolution of KBr at P_1. This point is termed a "primary saturation state" (for example, Glynn and others, 1990), which by definition lies on the solubility and solutus curve. The tie-line from P_1 on the solutus gives the composition of the solid in equilibrium with this solution composition, which may define the composition of the first precipitating solid. However, since the initial solid (here KBr) is still not in equilibrium it will dissolve further. The ongoing dissolution of KBr coupled with the precipitation of a mixed crystal shifts the aqueous solution on the solutus towards a more KBr-rich solution (left arrow in fig. 4). Accordingly, the composition of the precipitating solid must change continuously. Therefore, the composition of the solution and the solid will shift towards the dissolved component, here to higher $x_{Br,aq}$ and x_{KBr}^{repl} values, respectively. The end-point of this coupled dissolution-precipitation process, at which the initial crystal is completely dissolved and equilibrium between solution and precipitated solid has been reached,

can be determined by the lever-rule applied to the solubility phase diagram. It depends on the amount of substances in both solid and solution. A deduction of the lever-rule is given in Appendix A2.

Assuming an end-point at P_3 a mass balance of the reaction can be determined. The various dissolution-precipitation steps in which the solution closely follows the solubility/solutus curve can be summed up to give an *effective* path. This path only considers the dissolution of KBr and the precipitation of a solid which is in equilibrium with the solution at P_3. From the composition of the dissolving and precipitating component the (virtual) point P_2 can be derived and a mass balance equation can be written in accordance with equation (1):

$$AB + \frac{q(1 - x_{AB}^{repl})}{1 + (q-1)x_{AB}^{repl}} C^- \rightarrow \frac{q}{1 + (q-1)x_{AB}^{repl}} AB_{x_{AB}^{repl}}C_{1-x_{AB}^{repl}} + \left(1 - \frac{q}{1 + (q-1)x_{AB}^{repl}}\right)A^+ + \frac{1 - x_{AB}^{repl}}{1 + (q-1)x_{AB}^{repl}} B^-. \quad (14)$$

The derivation of this equation is based on the graphical representation of a general dissolution-precipitation pathway as shown in figure 3A and can be found in Appendix A3. Although not obvious at first glance, this formula is equivalent to the dissolution reaction given by Königsberger and Gamsjäger (1987, 1992) in their unified theory of solid solution solubility:

$$nAB_{x_0}C_{1-x_0} \rightarrow (n - \xi)AB_xC_{1-x} + [nx_0 - (n - \xi)x]B^- + [n(1 - x_0) - (n - \xi)(1 - x)]C^- + \xi A^+ \quad (15)$$

where n is the initial amount of the solid $AB_{x0}C_{1-x0}$. Equation (14) is formulated for n and x_0 equal to 1 and explicitly expresses the reaction extent variable as a function of q (which is a measure of the difference in solubility of the parent and product solid) and the composition of the replacement, x_{AB}^{repl}. The reaction extent variable is given by:

$$\xi = 1 - \frac{q}{1 + (q-1)x_{AB}^{repl}}. \quad (16)$$

In analogy to the system with no solid solution, the ΔV^r can be calculated using equation 3, but the ratio of precipitated to dissolved amount of substance now depends on the slope of the solubility curve $q = \left|\frac{\Delta m_{C,aq}}{\Delta m_{B,aq}}\right|$ between P_1 and P_3 as well as the composition of the replacement x_{AB}^{repl} as given by the mass balance (eq 14):

$$\frac{n_p}{n_d} = \frac{q}{1 + (q-1)x_{AB}^{repl}}. \quad (17)$$

Equation (3) can now be rewritten with equations (16) and (17) for a system with a solid solution as

$$\Delta V[\%] = \frac{n_p V_{M,p}}{n_d V_{M,d}} \cdot 100 - 100 = \frac{q}{1 + (q-1)x_{AB}^{repl}} \cdot \frac{V_{M,p}}{V_{M,d}} \cdot 100 - 100 = (1 - \xi)\frac{V_{M,p}}{V_{M,d}} \cdot 100 - 100. \quad (18)$$

Effectively, the ΔV^r calculation can be performed for different starting solutions and for any point on the solutus or solubility curve between P_1 and P_3 assuming a homogeneous replacement in equilibrium with the solution. Selected reaction paths

with their relative volume changes for a KBr crystal in a saturated KCl solution and KCl crystal in a saturated KBr solution have been summarized in table 1. Results for KBr and KCl crystals in mixed saturated solutions are given in figure 5 and will be described under "Volume change for Berthelot-Nernst precipitation" in more detail. Furthermore, both table 1 and figure 5 also contain information about a local volume change occurring at the reacting interface, which will be discussed under "Volume change for Doerner-Hoskins precipitation".

The underlying hypothesis for all reaction paths is that the composition of the precipitating solid is in equilibrium with the solution from which it is precipitating. Obviously, this is an oversimplification since supersaturation is needed as a driving force for crystallisation. As discussed by Astilleros and others (2003), a solid precipitating from a supersaturated solution (above the solutus) may not have the same composition as a solid forming in equilibrium with the solution (at the solutus). Furthermore, kinetic effects may arise during crystal growth, such as misfit strain at incoherent boundaries (Shtukenberg and others, 2006). However, a real reaction path must follow the solubility/solutus quite closely since there is a limit for overstepping the solubility (0.25 mol/l for KBr, 0.39 mol/l for KCl [Tovbin and Krasnova, 1951]) and, consequently, point P_2 in figure 3A, will never be reached in a real solution but only describes the effective path in terms of mass balance. Thus, it is not displayed in figure 4. Since our analysis only focuses on the general effect of the ΔV^r of the solid phase associated with difference in solubility for coupled dissolution-precipitation processes and its relevance for the textural evolution, such kinetic effects have been neglected at this stage.

Four different scenarios can be defined for dissolution-precipitation reactions in SS-AS system, which are limiting cases (table 2, fig. 6) as discussed by Glynn and others (1990):

1. In the **first** case the amount of solid is much greater than the amount of fluid. In this "solid controlled" scenario, the composition of a drop of solution, in the presence of a large volume of solid will change drastically while the solid will not noticeably change composition. Therefore, the position of the solid on the solidus defines the solution composition on the solutus by its tie-line. In terms of volume change of the solid phase this scenario is trivial since no significant change in solid composition also implies that there is no significant volume change.

2. Conversely, in the **second** scenario a small solid fragment in a large volume of solution will significantly change its composition while the solution composition will stay almost the same. In this "solution controlled" scenario the position of the solution on the solutus curve is fixed and defines the tie-line-connected replacement composition on the solidus curve. ΔV^r depends on the solubility and the molar volume of the involved solids and can be both positive or negative. Both scenarios describe closed system behavior where no transport of mass out of the system is allowed.

3. In a **third** scenario, an equilibrium end-point is also reached if the initial crystal has been reacted in part or completely and the compositionally homogeneous replacement is in equilibrium with the solution (upper reaction path in fig. 6), a situation which is analogous to Berthelot-Nernst precipitation (Berthelot, 1872; Nernst, 1891). The composition of this solid solution-aqueous solution pair depends on the initial solution to solid ratio and the initial compositions of solution and solid. It can be calculated by using the lever rule (Appendix A2) in connection with the solubility phase diagram. Most mineral solid solutions with moderate to high solubility will reach such an end-point over time. However, even for the KBr-KCl system, complete equilibration between a 2×2×1 mm solid KBr cube and solution needs about 2 hours(Putnis and others, 2005). Their experimental conditions are ideal to test the lever rule applied to a solubility phase diagram. Putnis and others (2005) used 17 mg

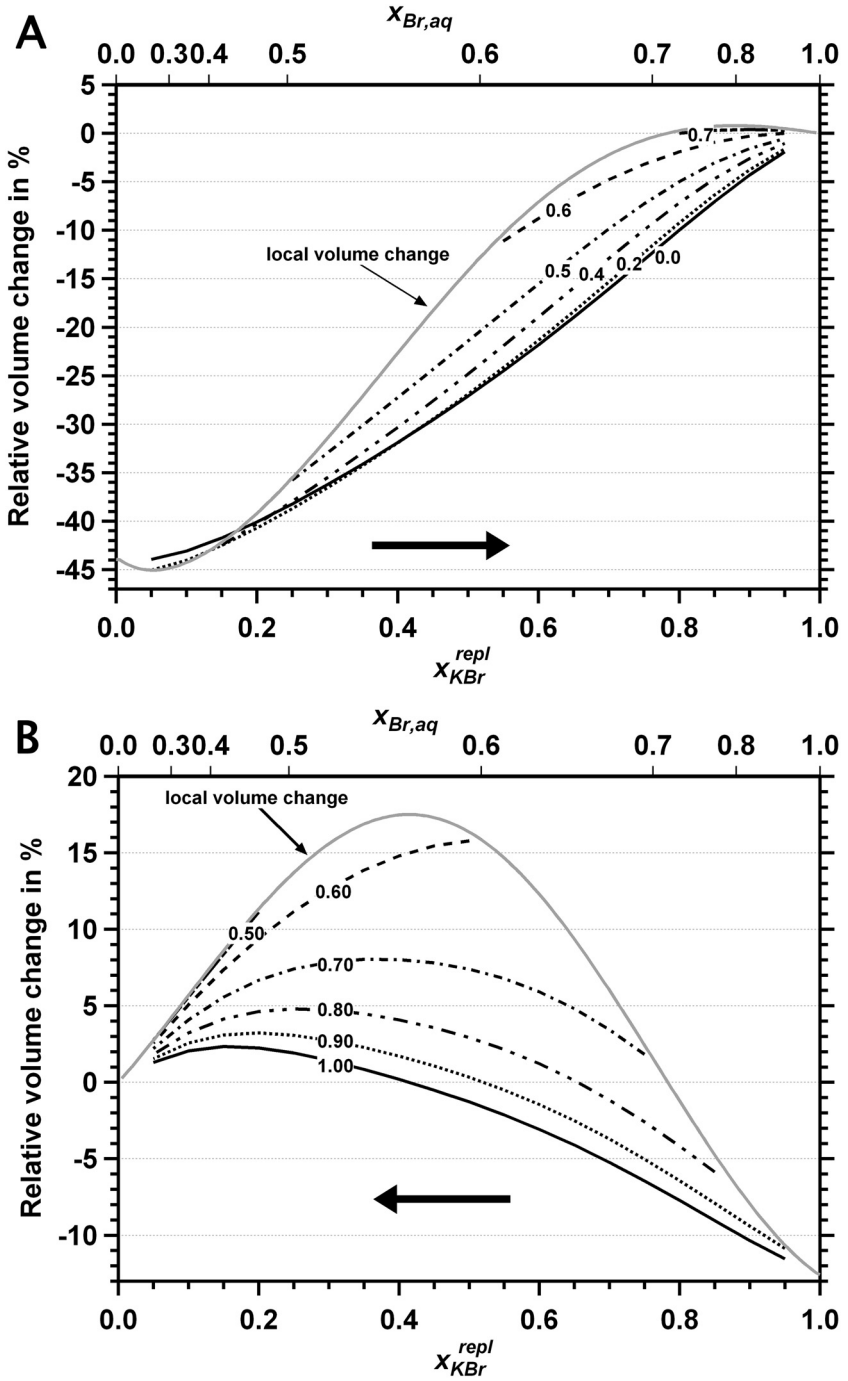

Fig. 5. Relative volume changes for KBr (A) and KCl (B) replaced in various solution compositions. The arrow indicates the evolution of the replacement and solution composition during reaction. The lower x-axis shows the composition of the replacement and the upper x-axis the corresponding solution composition in equilibrium. The initial solution composition $x_{Br,aq}$ is labelled on each curve. The volume change calculation for these curves assumes that the replacement is homogeneous in composition (Berthelot-Nernst precipitation, upper line in fig. 6). In contrast, the local volume change curve describes an envelope from which all reaction path dependent volume changes emerge (Doerner-Hoskins precipitation, lower line in fig. 6).

TABLE 2

Various scenarios defining end-points for dissolution-precipitation reactions in SS-AS systems

	Conditions	Controls on end-point	Controls on volume change	Geological conditions
Solid controlled	$n_{solution}/n_{solid} \rightarrow 0$	$x_{AB}^{init} \approx x_{AB}^{repl}$ x_{aq} @$t_0 \neq x_{aq}$ @t_2 x_{aq} will adjust according to x_{AB}^{init}	$q \rightarrow 0$ $V_{M,p}/V_{M,d} \rightarrow 1$ ΔV^r small	Closed system
Solution controlled	$n_{solution}/n_{solid} \rightarrow \infty$	$x_{AB}^{init} \neq x_{AB}^{repl}$ x_{aq} @$t_0 \approx x_{aq}$ @t_2 x_{AB}^{repl} will adjust according to x_{AB}^{init}	$q = \left\lvert \frac{\Delta m_{C^-}}{\Delta m_{B^-}} \right\rvert$, $V_{M,p}/V_{M,d}$ and ΔV^r variable	Solution dominated closed system; „Open“ system
Berthelot-Nernst precipitation	homogeneous replacement in equilibrium with solution	Defined by n^{tot} and x^{tot}; Can be calculated from the lever rule (see Appendix A3)	$q = \left\lvert \frac{\Delta m_{C^-}}{\Delta m_{B^-}} \right\rvert$, $V_{M,p}/V_{M,d}$ and ΔV^r variable	High solubility and/or reactivity, for example salt systems
Doerner-Hoskins precipitation	incremental layer of replacement in equilibrium with solution at time and place of precipitation	$x_{AB}^{init} \neq x_{AB}^{repl}$ x_{aq} @$t_0 \neq x_{aq}$ @t_1 Solution may not be homogeneous	$q(t) = \left\lvert \frac{\partial m_{C^-}}{\partial m_{B^-}} \right\rvert$, $V_{M,p}/V_{M,d}$ and ΔV^r variable	Low solubility and/or reactivity, for example silicates

KBr in a KCl saturated 250 μL solution, which is equivalent to 0.143 mmol KBr and 1.042 mmol KCl (using a solubility of 4.82 mol/kg H_2O and a density of 1.176 g/cm^3 for the saturated solution [Dejewska, 1993]). The calculated solid composition of the replaced crystal, x_{KBr}^{repl}, is 0.020, which is in excellent agreement with the measured value at the end of the experiment indicating that equilibrium had been reached.

4. A **fourth** scenario is equivalent to Doerner-Hoskins precipitation (Doerner and Hoskins, 1925). In this process, incremental layers of replacement are successively formed in local equilibrium with the solution at the reacting front, but the already replaced parts do not re-equilibrate with the evolving composition of the solution. In that case the replaced part is not homogeneous and only the last replaced part is in equilibrium with the bulk fluid. This scenario is important, because it may allow a qualitative estimate of the kinetics of an interface-coupled dissolution-precipitation reaction. Negative relative volume changes and the subsequent formation of porosity are a prerequisite for a relatively fast progression of a replacement front, because a solid of initial composition in disequilibrium with a solution will stay in contact with the solution through an interconnected porosity, formed at the reaction interface. However, positive volume changes prevent the formation of any porosity and can lead to a passivation of the initial crystal, which could stop or at least slow down the replacement process.

Volume change for Berthelot-Nernst precipitation.—The calculation of the ΔV^r is straightforward for this scenario because it assumes that the composition of the

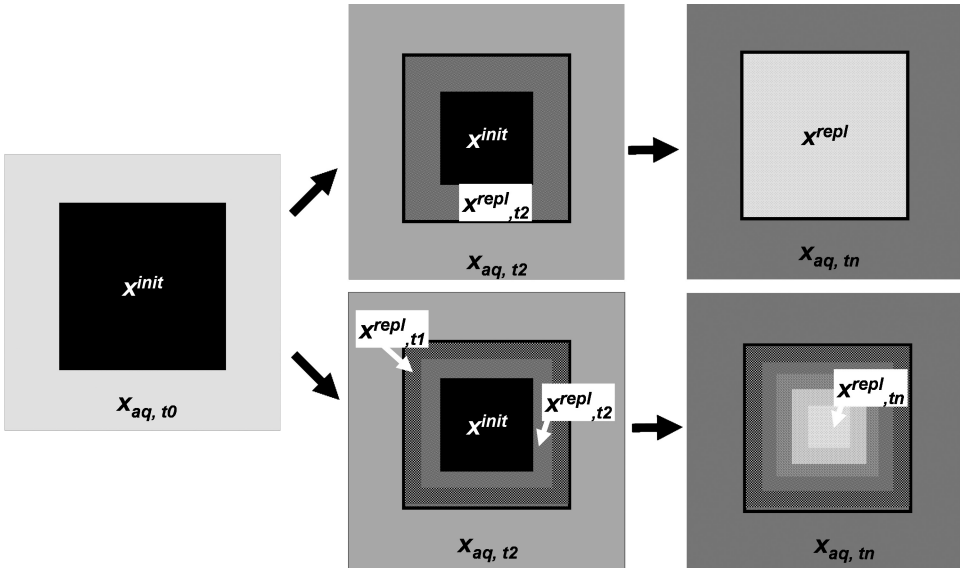

Fig. 6. Schematic reaction paths for Berthelot-Nernst (top) and Doerner-Hoskins (bottom) precipitation during mineral replacement (confer table 2).

replacement is linked to the solution composition at equilibrium (tie-line to point P_3 in fig. 4) on the solutus curve. Together with P_1, which is known from the starting conditions, the slope $q = \left|\frac{\Delta m_{C^-}}{\Delta m_{B^-}}\right|$ can be calculated. The mass balance (eq 14) can be used to calculate the amount of substance dissolved and precipitated and all calculations are based on 1 kg H_2O solvent and ΔV^r is deduced by equation (18). Thus, a systematic evaluation of the ΔV^r for different reaction paths can be easily performed by selecting both a starting fluid composition $x_{\mathrm{Br,aq}}$ and a resulting solid replacement composition x^{repl}_{KBr}. With equations (A15) and (A16) the coordinates of P_1 and P_3 can be calculated using the solutus and solidus expression for s_{eq}, respectively. Together with the slope q, the relative volume change ΔV^r is determined. Results from such a systematic approach are shown in figure 5. The figure shows ΔV^r as a function of the replacement composition x^{repl}_{KBr} and, on an upper x-axis, on the solution composition $x_{\mathrm{Br,aq}}$. Note that these scales are linked by the solidus and solutus expressions used for the Lippmann and solubility phase diagram (figs. 3B and 4, respectively). The calculation is based on the reaction of pure KBr (fig. 5A) and KCl (fig. 5B), respectively, in starting solutions of different compositions marked on each curve. The starting solutions are saturated, that is, they lie on the solutus and solubility curve, but they are not in equilibrium with the dissolving endmember (KBr or KCl). The composition of the replacement and the solution will evolve towards the dissolved component, that is, for the dissolution of KBr in pure KCl solution as an example, the solution as well as the replacement will become more Br-rich as the reaction proceeds. This evolution is denoted with an arrow in figure 5A and is equivalently applied to the reverse situation shown in figure 5B. For the calculation it is assumed that all of the dissolved amount of substance will mix with the entire solution and a solid in equilibrium with this solution will precipitate. Further dissolution then requires a continuous adjustment of the replacement composition.

Volume change for Doerner-Hoskins precipitation.—To determine the volume changes at the replacement front, the ΔV^r of infinitesimal small reaction steps must be

considered. This local volume change neglects all contributions of former dissolution-precipitation steps, which are integrated in Berthelot-Nernst precipitation. For infinitesimal small dissolution-precipitation steps points P_1 and P_3 (figs. 3A and 4) coincide and the local volume change depends directly on the slope of the solubility curve at this point, which is calculated by differentiating the solubility curve. Since we are considering a system that evolves continuously with time, this might be expressed as $\left(q(t) = \left|\frac{\partial m_{C^-}}{\partial m_{B^-}}\right|\right)$ (compare with the lower path in fig. 6). Equations (14) and (3) are used with all q(t) values (representing various solution compositions) determined from the differentiated solubility curve. Figure 5 shows that the local volume change represents a limiting case as all curves have to start from this local volume change curve. It thus gives an envelope curve for volume changes calculated for Berthelot-Nernst precipitation. The condition for Doerner-Hoskins precipitation may only be valid for very short time and length scales and dedicated experiments close to the zero volume change condition might be able to validate its relevance. Appropriate experimental conditions can be located by the use of the lever rule (Appendix A2) as described in the previous paragraph. It seems likely that Doerner-Hoskins precipitation is of increasing importance for less soluble systems such as silicates and therefore might be critical to understand fluid-mineral interaction and replacement under Earth crustal conditions. Computer-aided models that take account of both the thermodynamics and kinetics of reactions between complex rock-forming mineral solid solutions may be needed in such cases.

Dissolution of a thin layer of solid in a thin layer of fluid.—Between the two cases for precipitation discussed above and shown in figure 6 there is another scenario, which has already been shown to be relevant for replacement reactions in salt systems. As demonstrated by Putnis and others (2005), using real-time phase shift interferometry, the limited transport through the solution is measurable and steep compositional gradients develop at the reacting interface. Thus, for replacement reactions, the assumption of constant composition within the fluid phase during the precipitation is likely to be an oversimplification and neglects kinetic transport effects that may alter the composition of the solid crystallizing from a supersaturated solution.

As an example we assume a 10 nm thin layer of solid to be dissolved and mixed in a solution layer of defined thickness. For the purposes of illustration, we assume a surface area of 1 cm^2 in the calculation. The dissolution of a 10 nm layer of KBr will lead to a dissolved volume of KBr of 10^{-6} cm^3, which is equivalent to 2.75 μg KBr or 23.1 nmol KBr. If this amount of solid dissolves into a solution layer 1 μm thick of saturated KCl-solution (25 °C, 4.82 mol/kg H_2O), this solution volume of 10^{-3} cm^3 will contain 118 μg KCl solution (31 μg or 416 nmol of KCl) and 23.1 nmol KBr. Assumed that surface equilibrium is reached the resulting compositions would be $x_{KBr}^{repl} = 0.009$ for the solid and $x_{Br,aq} = 0.054$ for the solution. However, when a 10 nm layer is only mixed with a 100 nm solution layer, the compositions become significantly more Br-rich: $x_{KBr}^{repl} = 0.148$ and $x_{Br,aq} = 0.42$. The composition of the replacement and solution layer can be calculated for various ratios of thickness of the solution layer to thickness of dissolved layer as shown in figure 7. This mass balance calculation, based on the application of the lever rule (Appendix A2), highlights the importance of the transport and reaction kinetics for the composition of the replaced solid, as it can reach nearly any value of solid composition. However, it must be emphasized that a low dissolved solid to solution layer thickness ratio will lead to very high local supersaturation which in turn favors kinetically controlled precipitation.

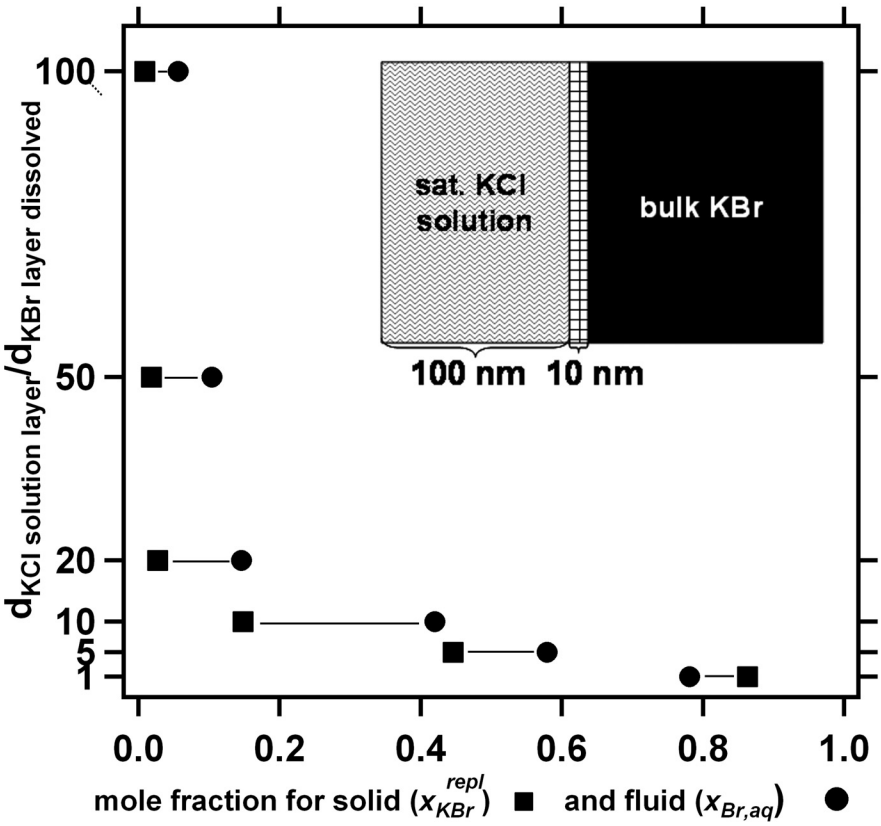

Fig. 7. Local equilibrium pairs for the reaction of a thin film in a layer of saturated KCl solution with a certain thickness together with a schematic drawing.

Comparison with Experimental Observations

As presented in the previous paragraphs, the ΔV^r caused by reactions in KBr-KCl-H_2O system is not constant, but depends on the reaction path, the fluid composition and the solid to fluid ratio. Both, negative and positive volume changes can occur under certain conditions and supposed reaction paths in this SS-AS system.

Here, we compare our theoretical analysis with available experimental data on replacement in the KBr-KCl-H_2O system (Putnis and Mezger, 2004; Putnis and others, 2005) and observations on newly performed experiments. Figure 8 illustrates the replacement of KBr in pure KCl solution (A-C) and the replacement of KCl in pure KBr solution (D-F).

KBr substrate in KCl solution.—In this first case, the negative ΔV^r is clearly visible as porosity in the replacement. The outlines of the larger pores are generally parallel to ⟨100⟩ and display the close orientational relationship between parent and replacement. Usually, finer pores are present next to the interface and this porosity coarsens towards the outside surface of the crystal. As observed by Putnis and others (2005), porosity can also partly or fully anneal out on the way to attaining textural equilibrium, which follows the chemical equilibration. The replacement rate is very fast (up to 40 μm/min) in the first 10 minutes of the experiment. The interface between the initial crystal and the replacement is usually wavy but shows a steep compositional gradient.

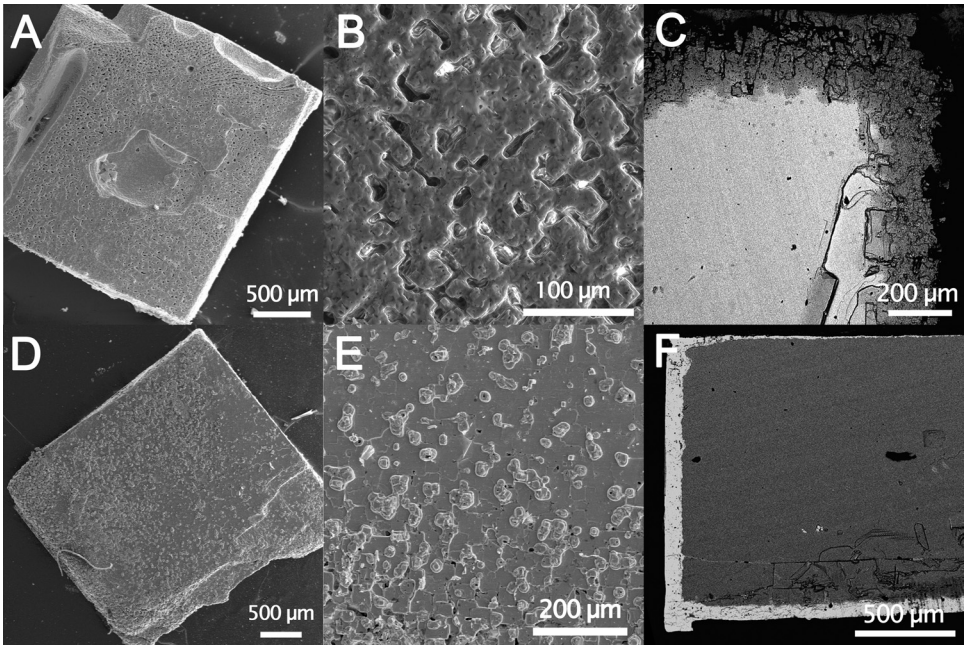

Fig. 8. Texture of a replaced surface of a KBr crystal in pure KCl solution (A, B, C) and a KCl crystal in pure KBr solution (D, E, F) after 25 minutes (for details of the experimental procedure see Putnis and Mezger, 2004). Secondary electron images (A, B, D, E) show porosity and growth hillocks indicating positive and negative volume change, respectively. The edges of the pores are generally crystallographically orientated with outlines parallel to the faces of the crystal, that is parallel to ⟨100⟩. Backscattered electron images (C, F) show a sharp compositional interface, which is wavy in case of negative volume changes (C) and straight with positive volume changes (F). Negative volume changes lead to a faster advancement of the reacting interface as porosity serves as a fluid pathway.

However, the most striking phenomenon is that the composition of the first precipitate is very Br-rich and becomes more Cl-rich during the reaction. This observation is apparently in contradiction with the reaction path inferred by solid solution-aqueous solution equilibrium, which predicts the first precipitate to be very chlorine-rich since a small amount of KBr mixes with the bulk KCl solution. The dissolution of a thin film of KBr in a limited KCl solution layer provides a reasonable explanation consistent with the real-time phase-shift interferometry results of Putnis and others (2005). With time, the solution starts to homogenize by diffusion within the fluid phase. The ratio between the solution layer thickness and the dissolved layer thickness starts to increase leading to a continuous shift of the replacement composition towards pure KCl. All of these "reaction sub-systems" have a negative ΔV^r that allow a fast progression of the replacement front and a complete replacement of KBr by KCl and chemical equilibration within about 2 hours as described before.

KCl substrate in KBr solution.—The reverse reaction shows significant differences in terms of reaction kinetics and the developed texture of the replacement. Generally, the replacement rate is much lower than for the replacement of KBr. For pure saturated KBr solution it can be up to 20 µm/min for the first 3 minutes, but then drops to less than 1 µm/min (Pollok, ms, 2005). The surface of the replaced KBr crystal shows some pores together with growth hillocks. These hillocks are small newly formed crystals that grow on top of the replaced surface and are interpreted as a consequence of a positive ΔV^r of the reaction. The interface is again very sharp but

much straighter than for the KBr replacement. The composition of the replacement, x^{repl}_{KBr}, is about 0.8 and, thus, very different from the initial composition (pure KCl). The replacement composition matches the composition at which the zero volume crossing of the local volume change curve from negative to positive ΔV^r occurs (fig. 5B). After an initial period of relatively fast replacement with negative volume change, which may have caused the residual porosity visible in figure 8E, the reacting surface will be sealed by the replacement, which significantly slows down the replacement rate. Further reaction requires diffusion at the replacement interface because the outer rim is in equilibrium with the surrounding solution but the non-replaced core is not. However any further evolution of the system leads to more positive ΔV^r values and material is precipitated onto the replaced surface as growth hillocks. For the replacement of KBr in a mixed KBr-KCl-saturated solution, the replacement rate is already very low at the start of the experiment since the local volume change at the interface will always be positive.

CONCLUSIONS AND IMPLICATIONS FOR MINERAL REPLACEMENT REACTIONS

In this paper, a model has been presented for quantitative analysis of volume change in a coupled dissolution-precipitation (replacement) reaction with special emphasis on SS-AS systems. The following conclusions can be drawn:

(1) A coupled dissolution-precipitation reaction can only form a pseudomorphic replacement if the associated negative ΔV^r is not too large. Percolation theory may help to define limiting porosity thresholds that depend on pore size and shape.
(2) ΔV^r is determined by both the molar volume of the solids in the dissolution-precipitation reaction *and* their relative solubility. This point may be of great importance for metamorphic reactions that are still often seen as isochemical reaction between minerals in a virtually closed system with fluid only acting as catalyst.
(3) The internal consistent combination of solubility diagram and solubility phase diagram allow to quantify ΔV^r for simple, but non-ideal SS-AS systems. More complex SS-AS systems involving rock-forming silicates necessitate direct computer-aided thermodynamic modeling involving solubility related volume changes.
(4) Relative volume changes in experiments depend strongly on the reaction path (Berthelot-Nernst versus Doerner-Hoskins precipitation or dissolution into finite solution layers). Additional information is therefore necessary to correctly predict ΔV^r and to make qualitative statement of the reaction rate.
(5) A further validation of these concepts for simple salt systems will require experiments with well defined solid to solution ratios, using the lever-rule together with a quantitative measurement of microporosity.

ACKNOWLEDGMENTS

We are grateful to Arkady Glikin who inspired the present work in the early stages. A number of people contributed by discussions on SS-AS systems: Jose Manuel Astilleros, Udo Becker, Thorsten Geisler, Hinrich Meyer, Carlos Pina, and Manuel Prieto. The authors thank Pierre Glynn and Dmitrii Kulik for carefully reviewing the paper and providing helpful comments. The study was funded by the Deutsche Forschungsgemeinschaft (PU153/5) and the BMBF in the GEOTECHNOLOGIEN programme "Mineral surfaces—from atomic processes to geotechnolgy" via the project MIMOS (publication no. GEOTECH-1527).

Appendix

A1 derivation of self-consistent solubility phase diagrams and solubility diagrams

Rewriting of equation (5) using $a_i = \gamma_i m_i$ leads to:

$$[A^+][B^-] = \gamma_{A^+}\gamma_{B^-} m_{A^+} m_{B^-} = K_{AB} x_{AB} f_{AB} \tag{A1}$$

$$[A^+][C^-] = \gamma_{A^+}\gamma_{C^-} m_{A^+} m_{C^-} = K_{AC} x_{AC} f_{AC}. \tag{A2}$$

Therefore, the molality of anions is:

$$m_{B^-} = \frac{K_{AB} x_{AB} f_{AB}}{\gamma_{A^+}\gamma_{B^-} m_{A^+}} \tag{A3}$$

$$m_{C^-} = \frac{K_{AC} x_{AC} f_{AC}}{\gamma_{A^+}\gamma_{C^-} m_{A^+}}. \tag{A4}$$

If equal molalities of cations and anions ($m_{A^+} = m_{B^-} + m_{C^-}$) are assumed, the molality of A^+ can be expressed as

$$m_{A^+} = \sqrt{\frac{K_{AB} x_{AB} f_{AB}}{\gamma_{A^+}\gamma_{B^-}} + \frac{K_{AC} x_{AC} f_{AC}}{\gamma_{A^+}\gamma_{C^-}}}. \tag{A5}$$

Referring to solutions saturated either with pure AB or AC lead to relationships of the end member solubilities s_{AB} and s_{AC}:

$$m^0_{A^+} m^0_{B^-} = \frac{K_{AB}}{\gamma^0_{A^+}\gamma^0_{B^-}} = s^2_{AB} \tag{A6}$$

$$m^0_{A^+} m^0_{C^-} = \frac{K_{AC}}{\gamma^0_{A^+}\gamma^0_{C^-}} = s^2_{AC}. \tag{A7}$$

To develop a connection between the molalities in the mixed solution and the solubility of the end members (that is between eqs (A3)–(A5) and eqs (A6) and (A7)) Azimov and Shtukenberg (2000) replaced the exponent 2 and $\gamma_i \neq \gamma_i^0$ in equations (A6) and (A7) by the empirical exponent Ψ and $\gamma_i = \gamma_i^0$. In this way an empirical correction for the differences in ionic strengths and the ion activities in pure and mixed solutions is applied:

$$(\sqrt{m_{A^+} m_{B^-}})^\Psi = \frac{K_{AB}}{\gamma_{A^+}\gamma_{B^-}} = s^\Psi_{AB} \tag{A8}$$

$$(\sqrt{m_{A^+} m_{C^-}})^\Psi = \frac{K_{AC}}{\gamma_{A^+}\gamma_{C^-}} = s^\Psi_{AC}. \tag{A9}$$

At equilibrium the molality of A^+ in the solution is equal to the total solubility with the assumption $m_{A^+} = m_{B^-} + m_{C^-}$. Rewriting equation (A5) with equation (A8) and (A9) results in an analogue to the solidus of the Lippmann model:

$$s^\Psi_{eq} = (\sqrt{m_{A^+}(m_{B^-} + m_{C^-})})^\Psi = s^\Psi_{AB} x_{AB} f_{AB} + s^\Psi_{AC} x_{AC} f_{AC} \tag{A10}$$

$$s_{eq} = m_{A^+,eq} = \sqrt[\Psi]{s^\Psi_{AB} x_{AB} f_{AB} + s^\Psi_{AC} x_{AC} f_{AC}}. \tag{A11}$$

The analogue for the solutus is:

$$s_{eq} = \sqrt[\Psi]{\frac{1}{\left(\frac{x_{B,aq}}{s^\Psi_{AB} f_{AB}} + \frac{x_{C,aq}}{s^\Psi_{AC} f_{AC}}\right)}}. \tag{A12}$$

The aqueous mole fractions are defined as

$$x_{B,aq} = \frac{m_{B^-}}{m_{B^-} + m_{C^-}} = \frac{s^\Psi_{AB} x_{AB} f_{AB}}{s^\Psi_{AB} x_{AB} f_{AB} + s^\Psi_{AC} x_{AC} f_{AC}} \tag{A13}$$

$$x_{C,aq} = \frac{m_{C^-}}{m_{B^-} + m_{C^-}} = \frac{\overset{\Psi}{s}_{AC} x_{AC} f_{AC}}{\overset{\Psi}{s}_{AB} x_{AB} f_{AB} + \overset{\Psi}{s}_{AC} x_{AC} f_{AC}}. \tag{A14}$$

The molalities of B and C at equilibrium are needed as x and y values to construct the solubility diagram from the solutus curve with internal consistency:

$$m_{B^-_{eq}} = x_{B,aq} s_{eq} \tag{A15}$$

$$m_{C^-_{eq}} = x_{C,aq} s_{eq}. \tag{A16}$$

A2 LEVER RULE AND ENDPOINTS

The application of the lever rule to the solubility phase diagram allows a prediction of the equilibrium composition and the amount of final precipitates and solution. The amount of substance as solid and in solution (n_{AB} and $n_{aq} = s_{eq}$, respectively) and the composition of coexisting solid and solution (x_{AB} and x_{aq}) can be determined from the total number of substances (n_{tot}) in the system and the composition of the total system (x_{tot}) by

$$n_{AB}(x_{tot} - x_{AB}) = n_{aq}(x_{aq} - x_{tot}). \tag{A17}$$

With $n_{AB} = n_{tot} - n_{aq}$ the equation can be rearranged to

$$x_{AB} = \frac{n_{aq} x_{aq} - n_{tot} x_{tot}}{n_{aq} - n_{tot}}. \tag{A18}$$

n_{aq} is the amount of substance in a saturated solution, that is, the solubility at a certain solution composition x_{aq} which is in equilibrium with a certain x_{AB}. This can be expressed by equation (A11), which is the solidus expression for the solubility phase diagram. x_{aq} is determined by equations (A13) and (A14). Therefore the former equation can be expressed as

$$x_{AB} = \frac{\sqrt[\Psi]{\overset{\Psi}{s}_{AB} x_{AB} f_{AB} + \overset{\Psi}{s}_{AC}(1 - x_{AB}) f_{AC}} \cdot \dfrac{\overset{\Psi}{s}_{AB} x_{AB} f_{AB}}{(\overset{\Psi}{s}_{AB} x_{AB} f_{AB} + \overset{\Psi}{s}_{AC}(1 - x_{AB}) f_{AC})} - n_{tot} x_{tot}}{\sqrt[\Psi]{\overset{\Psi}{s}_{AB} x_{AB} f_{AB} + \overset{\Psi}{s}_{AC}(1 - x_{AB}) f_{AC}} - n_{tot}} \tag{A19}$$

which can be solved iteratively.

A3 DERIVATION OF THE MASS BALANCE EQUATION

The mass balance equation for the coupled dissolution-precipitation reaction has been derived from the graphical representation of the reaction path as shown in figure 3A and figure A1. Note that the reaction path is a virtual one in order to mass balance the equations, but the real reaction is supposed to occur in multiple dissolution-precipitation steps close to the solubility line. The important assumption for the mass balance is the following: The precipitating solid at the end of the reaction is homogeneous and in equilibrium with the surrounding fluid. Thus, the hypothetical endpoint P_3 on the solubility curve defines the composition of the solid, which can be found from the connecting tie-line in a solubility-phase diagram.

The composition of the solid is given by $x_{AB}^{repl} = \dfrac{\Delta x}{\Delta x + \Delta y}$. With $\dfrac{1}{x_{AB}^{repl}} = \dfrac{\Delta x + \Delta y}{\Delta x} = 1 + \dfrac{\Delta y}{\Delta x}$ the slope between P_2 and P_3 can therefore be expressed as

$$\frac{|\Delta y|}{|\Delta x_{23}|} = \frac{1}{x_{AB}^{repl}} - 1. \tag{A20}$$

All distances are expressed as absolute values to avoid confusion regarding the denomination of points and the sign of coefficients.

For lengths of the dissolution path equal to 1, the segment $|\Delta x_{23}|$ can be determined in relation to the parameters q and x_{AB}^{repl}:

$$|\Delta x_{13}| + |\Delta x_{23}| = 1 \tag{A21}$$

$$q = \frac{|\Delta y|}{|\Delta x_{13}|} \tag{A22}$$

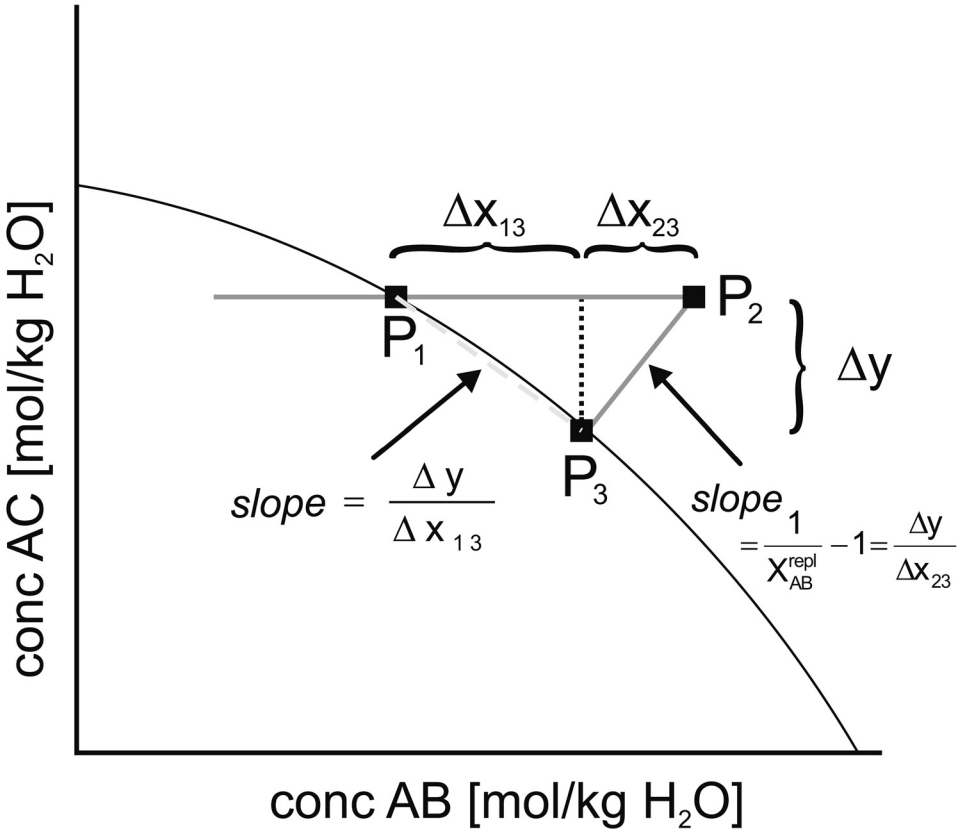

Fig. A1.

$$\frac{1}{x_{\mathrm{AB}}^{\mathrm{repl}}} - 1 = \frac{(1 - x_{\mathrm{AB}}^{\mathrm{repl}})}{x_{\mathrm{AB}}^{\mathrm{repl}}} = \frac{|\Delta y|}{|\Delta x_{23}|}. \tag{A23}$$

Identifying $|\Delta y|$ in equations (A22) and (A23) using equation (A21) gives:

$$(1 - |\Delta x_{23}|) \cdot q = |\Delta x_{23}| \cdot \frac{(1 - x_{AB}^{repl})}{x_{AB}^{repl}} \tag{A24}$$

which can be transformed to:

$$\frac{(1 - |\Delta x_{23}|)}{|\Delta x_{23}|} = \frac{1}{|\Delta x_{23}|} - 1 = \frac{(1 - x_{AB}^{repl})}{x_{AB}^{repl} \cdot q}. \tag{A25}$$

Solving for $|\Delta x_{23}|$ results in:

$$|\Delta x_{23}| = \frac{q \cdot x_{AB}^{repl}}{(1 + [q - 1] \cdot x_{AB}^{repl})}. \tag{A26}$$

The amount of precipitated material is given by:

$$|\Delta x_{23}| + |\Delta y| = \frac{q \cdot x_{AB}^{repl}}{(1 + [q - 1] \cdot x_{AB}^{repl})} + \frac{q \cdot x_{AB}^{repl}}{(1 + [q - 1] \cdot x_{AB}^{repl})} \cdot \frac{(1 - x_{AB}^{repl})}{x_{AB}^{repl}} = \frac{q}{(1 + [q - 1] \cdot x_{AB}^{repl})}. \tag{A27}$$

From this coefficient all others can be easily determined by mass balance or using the unified theory (eq 15) of Königsberger and Gamsjäger (1987, 1992).

References

Astilleros, J. M., Pina, C. M., Fernández-Díaz, L., and Putnis, A., 2003, Supersaturation functions in binary solid solution-aqueous solution systems: Geochimica et Cosmochimica Acta, v. 67, p. 1601–1608, doi:10.1016/S0016-7037(02)01166-3.

Azimov, P. Y., and Shtukenberg, A. G., 2000, Simulation of phase diagrams for water-salt systems with solid solutions: Russian Journal of Inorganic Chemistry, v. 45, p. 1302–1309.

Baker, D. R., Paul, G., Sreenivasan, S., and Stanley, H. E., 2002, Continuum percolation threshold for interpenetrating squares and cubes: Physical Review E, v. 66, 046136, doi:10.1103/PhysRevE.66.046136.

Berthelot, M., 1872, On the law which governs the distribution of a substance between two solvents: Annales de Chimie et Physique (in French), v. 26, p. 408–417.

Blum, J. R., 1843, Die Pseudomorphosen des Mineralreichs: Sttutgart, Schweizerbart'sche Verlagsbuchhandlung, 378 p. (in German).

Cartwright, I., 1997, Permeability generation and resetting of tracers during metamorphic fluid flow: implications for advection-dispersion models: Contributions to Mineralogy and Petrology, v. 129, p. 198–208, doi:10.1007/s004100050332.

Dejewska, B., 1993, Some physicochemical parameters of saturated ternary solutions of systems with mixed crystals in their solid phase: Crystal Research and Technology, v. 28, p. 697–705, doi:10.1002/crat.2170280521.

Doerner, H. A., and Hoskins, W. M., 1925, Co-precipitation of radium and barium sulfates: Journal of the American Chemical Society, v. 47, p. 662–675, doi:10.1021/ja01680a010.

Durham, G. S., Rock, E. J., and Frayn, S. F., 1953, Solid solution of the alkali halides. I. The systems KBr-KCl-H_2O, RbBr-RbCl-H_2O, RbBr-KBr-H_2O at 25 °C: Journal of the American Chemical Society., v. 75, p. 5792–5794, doi:10.1021/ja01119a007.

Engvik, A. K., Golla-Schindler, U., Berndt, J., Austrheim, H., and Putnis, A., 2009, Intragranular replacement of chlorapatite by hydroxy-fluor-apatite during metamorphism: Lithos, v. 112, p. 236–246, doi:10.1016/j.lithos.2009.02.005.

Farelo, F., von Brachel, G., and Offermann, H., 1993, Solid-liquid equilibria in the ternary system NaCl-KCl-H_2O: The Canadian Journal of Chemical Engineering, v. 71, p. 141–146, doi:10.1002/cjce.5450710119.

Ferry, J. M., 2000, Patterns of mineral occurrence in metamorphic rocks: American Mineralogist, v. 85, p. 1573–1588.

Geisler, T., Berndt, J., Meyer, H.-W., Pollok, K., and Putnis, A., 2004, Low-temperature aqueous alteration of crystalline pyrochlore: Correspondence between nature and experiment: Mineralogical Magazine, v. 68, p. 905–922, doi:10.1180/0026461046860230.

Geisler, T., Pöml, P., Stephan, T., Janssen, A., and Putnis, A., 2005a, Experimental observation of an interface-controlled pseudomorphic replacement reaction in a natural crystalline pyrochlore: American Mineralogist, v. 90, p. 1683–1687, doi:10.2138/am.2005.1970.

Geisler, T., Janssen, A., Scheiter, D., Stephan, T., Berndt, J., and Putnis, A., 2010, Aqueous corrosion of borosilicate glass under acidic conditions: A new corrosion mechanism: Journal of Non-Crystalline Solids, v. 356, p. 1458–1465, doi:10.1016/j.jnoncrysol.2010.04.033.

Geisler, T., Seydoux-Guillaume, A. M., Poeml, P., Golla-Schindler, U., Berndt, J., Wirth, R., Pollok, K., Janssen, A., and Putnis, A., 2005b, Experimental hydrothermal alteration of crystalline and radiation-damaged pyrochlore: Journal of Nuclear Materials, v. 344, p. 17–23, doi:10.1016/j.jnucmat.2005.04.009.

Geisler, T., Schaltegger, U., and Tomaschek, F., 2007, Re-equilibration of zircon in aqueous fluids and melts: Elements, v. 3, n. 1, p. 43–50, doi:10.2113/gselements.3.1.43.

Glikin, A. E., 2008, Polymineral-metasomatic crystallogenesis: New York, Springer, 312 p.

Glynn, P. D., 2000, Solid-solution solubilities and thermodynamics: Sulfates, carbonates and halides, *in* Alpers, C. N., Jambor, J. L, and Nordstrom, D. K., editors, Sulfate Minerals: Reviews in Mineralogy and Geochemistry, v. 40, p. 481–511, doi:10.2138/rmg.2000.40.10.

Glynn, P. D., and Reardon, E. J., 1990, Solid-solution aqueous-solution equilibria: thermodynamic theory and representation: American Journal of Science, v. 290, p. 164–201, doi:10.2475/ajs.290.2.164.

Glynn, P. D., Reardon, E. J., Plummer, L. N., and Busenberg, E., 1990, Reaction paths and equilibrium end-points in solid-solution aqueous-solution systems: Geochimica et Cosmochimica. Acta, v. 54, n. 2, p. 267–282, doi:10.1016/0016-7037(90)90317-E.

Guggenheim, E. A., 1937, The theoretical basis for Raoult's law: Transactions of the Faraday Society, v. 33, p. 151–159, doi:10.1039/tf9373300151.

Harlov, D. E., and Förster, H.-J., 2003, Fluid-induced nucleation of (Y+REE)-phosohate minerals within apatite: Nature and experiment. Part II. Fluoroapatite: American Mineralogist, v. 88, p. 1209–1229.

Harlov, D. E., Förster, H.-J., and Nijland, T. G., 2002, Fluid-induced nucleation of (Y+REE)-phosphate minerals within apatite: Nature and experiment—Part I. Chlorapatite: American Mineralogist, v. 87, p. 245–261.

Harlov, D. E., Wirth, R., and Förster, H.-J., 2005, An experimental study of dissolution-reprecipitation in fluorapatite: Fluid infiltration and the formation of monazite: Contributions to Mineralogy and Petrology, v. 150, n. 3, p. 268–286, doi:10.1007/s00410-005-0017-8.

Hövelmann, J., Putnis, A., Geisler, T., Schmidt, B. C., and Golla-Schindler, U., 2010, The replacement of plagioclase feldspars by albite: observations from hydrothermal experiments: Contributions to Mineralogy and Petrology, v. 159, n. 1, p. 43–59, doi:10.1007/s00410-009-0415-4.

Jamtveit, B., Austrheim, H., and Malthe-Sørenssen, A., 2000, Accelerated hydration of the Earth's deep crust induced by stress perturbations: Nature, v. 408, p. 75–79, doi:10.1038/35040537.

Königsberger, E., and Gamsjäger, H., 1987, Solid-solute phase equilibria in aqueous solution—I. Solubility constant and free enthalpy of formation of huntite: Berichte der Bunsengesellschaft für Physikalische Chemie, v. 91, p. 785–790.

——— 1992, Comment: Solid-solution aqueous-solution equilibria: thermodynamic theory and representation: American Journal of Science, v. 292, p. 199–214, doi:10.2475/ajs.292.3.199.

Kulik, D. A., 2006, Dual-thermodynamic estimation of stoichiometry and stability of solid solution end members in aqueous-solid solution systems: Chemical Geology, v. 225, n. 2–3, p. 189–212, doi:10.1016/j.chemgeo.2005.08.014.

Kusiak, M. A., Dunkley, D. J., Słaby, E., Martin, H., and Budzyń, B., 2009, Sensitive high-resolution ion microprobe analysis of zircon reequilibrated by late magmatic fluids in a hybridized pluton: Geology, v. 37, n. 12, p. 1063–1066, doi:10.1130/G30048A.1.

Labotka, T. C., Cole, D. R., Fayek, M., Riciputi, L. R., and Staderman, F. J., 2004, Coupled cation and oxygen-isotope exchange between alkali feldspar and aqueous chloride solution: American Mineralogist, v. 89, n. 11–12, p. 1822–1825.

Lippmann, F., 1977, The solubility product of complex minerals, mixed crystals and three-layer clay minerals: Neues Jahrbuch für Mineralogie—Abhandlungen, v. 130, p. 243–263.

——— 1980, Phase diagrams depicting the aqueous solubility of mineral systems: Neues Jahrbuch für Mineralogie—Abhandlungen, v. 139, p. 1–25.

——— 1982, Stable and metastable solubility diagrams for the system $CaCO_3$-$MgCO_3$-H_2O at ordinary temperature: Bulletin de Mineralogie, v. 105, p. 273–279.

Nernst, W., 1891, Distribution of a substance between two solvents and between solvents and vapor: Physical Chemistry, v. 8, p. 110–139.

Niedermeier, D. R. D., Putnis, A., Geisler, T., Golla-Schindler, U., and Putnis, C. V., 2009, The mechanism of cation and oxygen isotope exchange in alkali feldspars under hydrothermal conditions: Contributions to Mineralogy and Petrology, v. 157, n. 1, p. 65–76, doi:10.1007/s00410-008-0320-2.

O'Neil, J. R., and Taylor, H. P., 1967, The oxygen isotope and cation exchange chemistry of feldspars: American Mineralogist, v. 52, p. 1414–1437.

Parsons, I., and Lee, M. R., 2009, Mutual replacement reactions in alkali feldspars I: microtextures and mechanisms: Contributions to Mineralogy and Petrology, v. 157, n. 5, p. 641–661, doi:10.1007/s00410-008-0355-4.

Plummer, L. N., Parkhurst, D. L., Fleming, G. W., and Dunkle, S. A., 1988, A computer program incorporating Pitzer's equations for calculation of geochemical reactions in brines: U.S. Geological Survey, Water Resources Investigations Report 88–4153, 310 p.

Pollok, K., ms, 2005, Crystal growth patterns in solid solution systems: Case studies on oscillatory zoning and mineral replacement reactions: Münster, Germany, WestfälischeWilhelms-Universität Münster, Ph. D. thesis, p. 146, http://miami.uni-muenster.de/servlets/DerivateServlet/Derivate-3624/diss_pollok.pdf

Pollok, K., Lloyd, G. E., Austrheim, H., and Putnis, A., 2008, Complex replacement patterns in garnets from Bergen Arcs eclogites: A combined EBSD and analytical TEM study: Chemie der Erde—Geochemistry, v. 68, n. 2, p. 177–191, doi:10.1016/j.chemer.2007.12.002.

Prieto, M., 2009, Thermodynamics of solid solution-aqueous solution systems: Reviews in Mineralogy and Geochemistry, v. 70, n. 1, p. 47–85, doi:10.2138/rmg.2009.70.2.

Putnis, A., 2002, Mineral replacement reactions: from macroscopic observations to microscopic mechanisms: Mineralogical Magazine, v. 66, p. 689–708 doi:10.1180/0026461026650056.

——— 2009, Mineral replacement reactions: Reviews in Mineralogy and Geochemistry, v. 70, n. 1, p. 87–124, doi:10.2138/rmg.2009.70.3.

Putnis, A., and John, T., 2010, Replacement processes in the Earth's crust: Elements, v. 6, n. 3, p. 159–164, doi:10.2113/gselements.6.3.159.

Putnis, A., and Putnis, C. V., 2007, The mechanism of reequilibration of solids in the presence of a fluid phase: Journal of Solid State Chemistry, v. 180, n. 5, p. 1783–1786, doi:10.1016/j.jssc.2007.03.023.

Putnis, A., Putnis, C. V., and Giampaolo, C., 1994, The microstructure of analcime phenocrysts in igneous rocks: European Journal of Mineralogy, v. 6, p. 627–632.

Putnis, A., Prieto, M., and Fernandez-Diaz, L., 1995, Fluid supersaturation and crystallization in porous media: Geological Magazine, v. 132, p. 1–13, doi:10.1017/S0016756800011389.

Putnis, A., Hinrichs, R., Putnis, C. V., Golla-Schindler. U., and Collins, L. G., 2007a, Hematite in porous red-clouded feldspar: Evidence of large-scale crustal fluid-rock interaction: Lithos, v. 95, n. 1–2, p. 10–18, doi:10.1016/j.lithos.2006.07.004.

Putnis, C. V., and Mezger, K., 2004, A mechanism of mineral replacement: Isotope tracing in the model system KCl-KBr-H_2O: Geochimica et Cosmochimica Acta, v. 68, n. 13, p. 2839–2848, doi:10.1016/j.gca.2003.12.009.

Putnis, C. V., Tsukamoto, K., and Nishimura, Y., 2005, Direct observation for pseudomorphism: Compositional and textural evolution at a fluid-solid interface: American Mineralogist, v. 90, n. 11–12, p. 1909–1912, doi:10.2138/am.2005.1990.

Putnis, C. V., Geisler, T., Schmid-Beurmann, P., Stephan, T., and Giampaolo, C., 2007b, An experimental study of the replacement of leucite by analcime: American Mineralogist, v. 92, n. 1, p. 19–26, doi:10.2138/am.2007.2249.

Ramdohr, P., 1980, The ore minerals and their intergrowths: Oxford, Pergamon Press, 1205 p.

Redlich, O., and Kister, A. T., 1948, Algebraic representation of thermodynamic properties and the classification of solutions: Industrial and Engineering Chemistry, v. 40, p. 345–348, doi:10.1021/ie50458a036.

Rendón-Angeles, J. C., Yanagisawa, K., Ishizawa, N., and Oishi, S., 2000a, Conversion of calcium fluoroapatite into calcium hydroxyapatite under alkaline hydrothermal conditions: Journal of Solid State Chemistry, v. 151, n. 1, p. 65–72, doi:10.1006/jssc.1999.8623.

——— 2000b, Topotaxial conversion of chloroapatite and hydroxyapatite to fluorapatite by hydrothermal ion exchange: Chemistry of Materials, v. 12, p. 2143–2150, doi:10.1021/cm990797x.

——— 2000c, Effect of metal ions of chloroapatites on the topotaxial replacement by hydroxyapatite under hydrothermal conditions: Journal of Solid State Chemistry, v. 154, p. 569–578, doi:10.1006/jssc.2000.8888.

Rubatto, D., Müntener, O., Barnhoorn, A., and Gregory, C., 2008, Dissolution-reprecipitation of zircon at low-temperature, high-pressure conditions (Lanzo Massif, Italy): American Mineralogist, v. 93, 1519–1529, doi:10.2138/am.2008.2874.

Rumble, D., III, and Spear, F. S., 1983, Oxygen isotope equilibration and permeability enhancement during regional metamorphism: Journal of the Geological Society, v. 140, p. 619–628, doi:10.1144/gsjgs.140.4.0619.

Seydoux-Giullaume, A.-M., Wirth, R., and Ingrin, J., 2007, Contrasting response of $ThSiO_4$ and monazite to natural irridation: European Journal of Mineralogy, v. 19, n. 1, p. 7–14, doi:10.1127/0935-1221/2007/0019-007.

Shtukenberg, A. G., Punin, Y. O., and Azimov, P., 2006, Crystallization kinetics in binary solid solution-aqueous solution systems: American Journal of Science, v. 306, p. 553–574, doi:10.2475/07.2006.03.

Silcock, H. L., editor, 1979, Solubilities of Inorganic and Organic Compounds: Oxford, Pergamon Press, v. 3, 499 p.

Soman, A., Geisler, T., Tomaschek, F., Grange, M., and Berndt, J., 2010, Alteration of crystalline zircon solid solutions: a case study on zircon from an alkaline pegmatite from Zomba-Malosa, Malawi: Contributions to Mineralogy and Petrology, v. 160, n. 6, p. 909–930, doi 10.1007/s00410-010-0514-2.

Spandler, C., Hermann, J., and Rubatto, D., 2004, Exsolution of thortveitite, yttrialite, and xenotime during low-temperature recrystallization of zircon from New Caledonia, and their significance for trace element incorporation in zircon: American Mineralogist, v. 89, n. 11–12, p. 1795–1896.

Tenailleau, C., Pring, A., Etschmann, B., Brugger, J., Grguric, B. A., and Putnis, A., 2006, Transformation of pentlandite to violarite under mild hydrothermal conditions: American Mineralogist, v. 91, p. 706–709, doi:10.2138/am.2006.2131.

Tomaschek, F., Kennedy, A. K., Villa, I. M., Lagos, M., and Ballhaus, C., 2003, Zircons from Syros, Cyclades, Greece—recrystallization and mobilization of zircon during high-pressure metamorphism: Journal of Petrology, v. 44, p. 1977–2002, doi:10.1093/petrology/egg067.

Tovbin, M. V., and Krasnova, S. I., 1951, Stability of supersaturated solutions of salts: Russian Journal of Physical Chemistry A, v. 25, p. 161–166 (in Russian).

Walker, F. D. L., Lee, M. R., and Parsons, I., 1995, Micropores and micropermeable texture in alkali-feldspars: geochemical and geophysical implications: Mineralogical Magazine, v. 59, n. 3, p. 505–534, doi:10.1180/minmag.1995.059.396.12.

Xia, F., Brugger, J., Chen, G., Ngothai, Y., O'Neill, B., Putnis, A., and Pring, A., 2009, Mechanism and kinetics of pseudomorphic mineral replacement reactions: A case study on the replacement of pentlandite by violarite: Geochimica et Cosmochimica Acta, v. 73, n. 7, p. 1945–1969, doi:10.1016/j.gca.2009.01.007.

Yanagisawa, K., Rendón-Angeles, J. C., Ishizawa, N., and Oishi, S., 1999, Topotaxial replacement of chloroapatite by hydroxyapatite during hydrothermal ion exchange: American Mineralogist, v. 84, n. 11–12, p. 1861–1869.